A local radial basis function collocation method for band structure computation of phononic crystals with scatterers of arbitrary geometry

ZHENG, HUI, Yang, Z, Zhang, C & Tyrer, M

Original citation & hyperlink:
ZHENG, HUI, Yang, Z, Zhang, C & Tyrer, M 2018, 'A local radial basis function collocation method for band structure computation of phononic crystals with scatterers of arbitrary geometry' *Applied Mathematical Modelling*, vol 60, pp. 447-459
https://dx.doi.org/10.1016/j.apm.2018.03.023

DOI 10.1016/j.apm.2018.03.023
ISSN 0307-904X

Publisher: Elsevier

A local radial basis function collocation method for band structure computation of phononic crystals with scatterers of arbitrary geometry

H. Zheng[1,2], Z. Yang[2,*], Ch. Zhang[3], M. Tyrer[2]

[1]School of Civil Engineering And Architecture, Nanchang University, 330031, China

[2]Centre for Low Impact Buildings, Coventry University, CV1 5FB, United Kingdom

[3]Department of Civil Engineering, University of Siegen, D-57068 Siegen, Germany

Abstract: A numerical algorithm based on the local radial basis function collocation method (LRBFCM) is developed for the efficient computation of the derivatives of the primary field quantities. Instead of a direct calculation of the derivatives by using the partial differentiation of the shape functions as in the traditional numerical approach, the derivative calculation in the present work is performed by using a simple finite difference scheme with an introduced fictitious node. The developed algorithm is very geometrically flexible and can be easily applied to the continuity and boundary conditions of arbitrary geometries, which require an accurate derivative computation of the primary field quantities. Based on the present numerical approach, the developed LRBFCM has been applied to the phononic crystals with scatterers of an arbitrary geometry, which has not yet been reported before to the authors' knowledge. A few examples for anti-plane elastic wave propagation are modelled to validate the developed LRBFCM. A comparison with finite element modelling shows that the present method is efficient and flexible.

Keywords: Phononic crystals, interface conditions, elastic wave propagation, band structures, eigenvalue problems, radial basis functions.

1. Introduction

Acoustic or elastic waves of a certain range of frequencies cannot propagate in periodic structures due to the periodic variation of material properties [1]. In order to evaluate the bandgaps that stop the wave propagation, different numerical methods have been applied to compute the band structures of phononic crystals, but most of the existing methods cannot efficiently undertake this challenging task. For example, a large number of elements are needed to ensure the continuity and the equilibrium conditions on solid-fluid interfaces when the conventional FEM is used [3-5]. Neglecting transverse waves in the solid parts might result in high numerical errors in the plane wave expansion method [6, 7] and the wavelet method [8, 9]. The multi-scattering theory method [10, 11] and the Dirichlet-to-Neumann map method [12, 13] are only suitable for scatterers with simple shapes such as circles and spheres. The boundary element method (BEM) [15, 16] involves singular integrals and may result in fictitious eigenfrequencies or missing of some eigenfrequencies. The generalized multipole technique [16, 17] is computationally very demanding because the band structure can only be obtained from the time domain using the Fast Fourier Transform method. The time-domain finite difference approach [18, 19] is able to consider different wave modes in solids and fluids but often has to neglect solid-fluid interactions at the interfaces. Therefore, accurate and efficient numerical methods are still needed to compute the band structures of phononic crystals.

The meshless method of the radial basis function collocation method (RBFCM) has been developed many years [23-25]. Due to the full matrix formulated in the RBFCM, the single local collocation approach is introduced, which is also known as the RBF-FD method or local RBFCM (LRBFCM) [26-30]. However, the instability caused by the Neumann boundary conditions limits its wider applications considerably [27, 31]. In order to solve this problem, special treatments were introduced to the LRBFCM for the derivation calculation. The fictitious nodes are introduced near the boundaries to increase the smooth of the solution and avoid of one side stencil [32, 33], however the fictitious nodes increase the size of the formulated matrix, and might have a limitation in the application of multi-domian eigenvalue problems; The least square method is introduced to develop LRBFCM to the phononics crystals [34, 35], but the only considered case is limited in the square lattice with square scatterers, the instability of the derivative calculation is still remain unsolved. The direct method, indirect method and fictitious node method were proposed for the derivative calculation in LRBFCM, and have been applied to phononic crystals of different problems [36-38]. However, these methods are still not easy to be applied to the phononic crystals with a complex geometry interface. By far, the LRBFCM has not yet been applied to the phononic crystals with a complex scatterer before.

In this work, a simple approach is introduced in the LRBFCM to deal with the instability caused by derivative calculation. Unlike other finite difference form introduced in LRBFCM [27, 39], the derivative calculation in this presented work is evaluated by using a simple finite difference form between the source point and one introduced fictitious node, the derivative of any direction at any node can be easily evaluated. The introduced fictitious node does not increase the size of the formulated matrix, and can greatly increase the geometric flexibility of the LRBFCM. A boundary value problem is first introduced to present the stability of this new approach. The improved LRBFCM is then applied to compute the band structures of phononic crystals with scatterers of arbitrary geometry. Two examples with anti-plane elastic wave propagation were modelled using the improved method and the results were compared by FEM models. The paper is organized as follows. The general form of LRBFCM and the new numerical technique is given in section 2. The stability tests with a boundary value problem is given in the section 3. The problem of phononic crystals are briefly introduced in section 4. The numerical results of the phononic crystals are presented and discussed in section 5, followed by some conclusions in the last section.

2. LRBFCM and the numerical technique for derivative calculation

2.1 General formulation of LRBFCM

In the LRBFCM formulation, the general solution of the field quantity u is approximated by

$$u(\boldsymbol{x}) = \sum_{m=1}^{N_s} \varphi\left(\left\|\boldsymbol{x} - \boldsymbol{x}_m\right\|\right)\alpha_m \,, \tag{1}$$

where N_s is the total number of local nodes, $\boldsymbol{\varphi}$ the RBF, and α_m the unknown coefficient related to $u(\boldsymbol{x}_m)$ of the local node at $\boldsymbol{x}_m$, which can be calculated by

$$\boldsymbol{\alpha}_m = \boldsymbol{\varphi}^{-1}\overline{\boldsymbol{u}}, \tag{2}$$

where $\overline{\boldsymbol{u}} = [u(\boldsymbol{x}_1), \ldots, u(\boldsymbol{x}_m)]^T$ is the vector of the field quantities of the local nodes (m=1, N_s), $\boldsymbol{\alpha}_m = [\alpha_1, \alpha_2, \ldots, \alpha_m]^T$ is the vector of unknown coefficients, and $\boldsymbol{\varphi} = \left[\varphi\left(\left\|\boldsymbol{x}_j - \boldsymbol{x}_l\right\|\right)\right]_{1 \le l, j \le N_s}$ is the RBF interpolation matrix with the size of $N_s \times N_s$.

Considering Eq. (1), Eq. (2) can be expressed as

$$u(\boldsymbol{x}) = \sum_{m=1}^{N_s} \varphi\left(\left\|\boldsymbol{x} - \boldsymbol{x}_m\right\|\right)\alpha_m = \boldsymbol{\Theta}\boldsymbol{\varphi}^{-1}\overline{\boldsymbol{u}}, \tag{3}$$

where

$$\boldsymbol{\Theta} = \left[\varphi\left(\left\|\boldsymbol{x} - \boldsymbol{x}_1\right\|\right), \ldots, \varphi\left(\left\|\boldsymbol{x} - \boldsymbol{x}_{N_s}\right\|\right)\right]. \tag{4}$$

In Eq. (3), $\boldsymbol{\Theta}\boldsymbol{\varphi}^{-1}$ is the vector with the size of N_s that relates to local nodes. For convenience, the following definition is introduced

$$\overline{\boldsymbol{\varphi}}(\boldsymbol{x}) = \boldsymbol{\Theta}(\boldsymbol{x})\boldsymbol{\varphi}^{-1}. \tag{5}$$

Then the field quantities given in Eq. (3) can be expressed as

$$u(\boldsymbol{x}) = \overline{\boldsymbol{\varphi}}(\boldsymbol{x})\overline{\boldsymbol{u}}. \tag{6}$$

From Eq. (6), it is easy to reformulate the vector $\overline{\boldsymbol{\varphi}}(\boldsymbol{x})$ to a global vector by inserting zeros at proper positions. For simplicity, two global vectors $\tilde{\boldsymbol{\varphi}}(\boldsymbol{x})$ and $\tilde{\boldsymbol{u}}$ with the size of N (the number of global nodes) are defined by mapping the local ones with the size of N_s as

$$\begin{aligned} &\text{local } \overline{\boldsymbol{\varphi}}(\boldsymbol{x}) \quad \Rightarrow \quad \text{global } \tilde{\boldsymbol{\varphi}}(\boldsymbol{x}), \\ &\text{local } \overline{\boldsymbol{u}} \quad \Rightarrow \quad \text{global } \tilde{\boldsymbol{u}}, \end{aligned} \tag{7}$$

where $\tilde{\boldsymbol{u}} = [u(\boldsymbol{x}_1), \ldots, u(\boldsymbol{x}_N)]^T$ is the vector of field quantities in the global domain. The global vector $\tilde{\boldsymbol{\varphi}}(\boldsymbol{x}) = [\tilde{\varphi}_1(\boldsymbol{x}), \ldots, \tilde{\varphi}_N(\boldsymbol{x})]$ is a sparse vector related to the local vector. Using the relationships (7), Eq. (6) can be expressed as

$$u(\boldsymbol{x}) = \overline{\boldsymbol{\varphi}}(\boldsymbol{x})\overline{\boldsymbol{u}} = \tilde{\boldsymbol{\varphi}}(\boldsymbol{x})\tilde{\boldsymbol{u}}, \tag{8}$$

where the unknown field quantity vector $\tilde{\boldsymbol{u}}$ can be determined from governing partial differential equations and boundary conditions. $\overline{\boldsymbol{\varphi}}(\boldsymbol{x})$ is related to the the partial differentiation of $\Theta(\boldsymbol{x})$ while $\boldsymbol{\varphi}^{-1}$ is a constant matrix, i.e.,

$$\frac{\partial u(\boldsymbol{x})}{\partial x_i} = \frac{\partial \tilde{\boldsymbol{\varphi}}(\boldsymbol{x})}{\partial x_i}\tilde{\boldsymbol{u}} \;\Rightarrow\; \frac{\partial \overline{\boldsymbol{\varphi}}(\boldsymbol{x})}{\partial x_i}\overline{\boldsymbol{u}} = \frac{\partial \boldsymbol{\Theta}(\boldsymbol{x})}{\partial x_i}\boldsymbol{\varphi}^{-1}\overline{\boldsymbol{u}}, \tag{9}$$

The function $\tilde{\boldsymbol{\varphi}}(\mathbf{x})$ obeys the Kronecker-delta property, $\tilde{\varphi}_k(\boldsymbol{x}_m) = \delta_{km}$ or $\tilde{\boldsymbol{\varphi}}(\boldsymbol{x}_m) = [\tilde{\varphi}_1(\boldsymbol{x}_m) = 0, \ldots, \tilde{\varphi}_m(\boldsymbol{x}_m) = 1, \ldots, \tilde{\varphi}_N(\boldsymbol{x}_N) = 0]$ and hence

$$u(x_m) = \tilde{\boldsymbol{\varphi}}(\boldsymbol{x}_m)\tilde{\boldsymbol{u}} = \sum_{k=1}^{N} \tilde{\varphi}_k(\boldsymbol{x}_m)u(\boldsymbol{x}_k) = \sum_{k=1}^{N} \delta_{km}u(\boldsymbol{x}_k) = u(\boldsymbol{x}_m), \tag{10}$$

where the subscript *m* denotes the *m*th element of a vector, the corresponding field quantity at the *m*th node $\boldsymbol{x} = \boldsymbol{x}_m$.

2.2 The numerical technique for derivative calculation

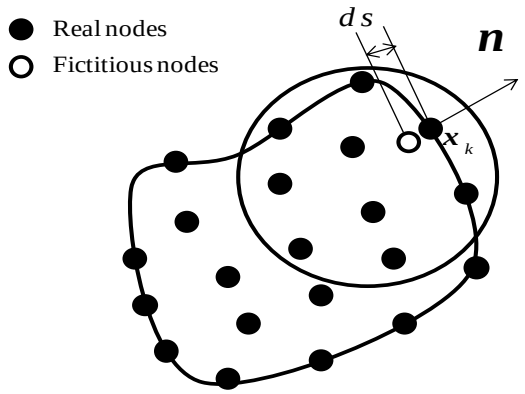

Fig. 1 The improved fictitious node method

The instabilities of the LRBFCM may stop the application of the LRBFCM. Many numerical approaches, such as residual based error [40,41], least-squares method [42,43], have been applied to deal with the instability of the collocation method [44, 45]. Instabilities of the LRBFCM may relate to shape parameter, local nodes, nodes distribution and so on. One of the key instabilies caused by the LRBFCM is the derivative calculation. In the proposed numerical approach of solving derivative, a fictitious node or *ghost node* is used as shown in Fig. 1. This fictitious node is interpolated by using the local nodes, and thus does not increase the size of the formulated matrix. The derivative of $\partial u / \partial \boldsymbol{n}$ can be calculated in two steps. Firstly, the field quantity values on the fictitious node is interpolated using the information of the real nodes nearby, as shown in the circular area in Fig. 1. Hence we have

$$u(\tilde{\boldsymbol{x}}) = \tilde{\boldsymbol{\varphi}}(\tilde{\boldsymbol{x}})\boldsymbol{u}_{N_s}, \tag{11}$$

where $\boldsymbol{u}_{N_s} = [u(\boldsymbol{x}_1), \ldots, u(\boldsymbol{x}_{N_s})]^T$ are the values of the field quantities at real nodes in the local domain, and $\tilde{\boldsymbol{x}}$ is the fictitious node that does not exist in the reality. Then the derivative can be

formulated using a finite difference form instead of the RBF trial function, by subtracting the field quantity of the source node $\boldsymbol{x}_k$. The derivative of the field quantity can be expressed as

$$\frac{\partial u(\boldsymbol{x})}{\partial \boldsymbol{n}} = \frac{u(\boldsymbol{x}) - u(\tilde{\boldsymbol{x}})}{ds}, \tag{12}$$

where *ds* is the distance between the source node and the fictitious node, as shown in Fig. 3. Considering Eqs. (10) and (11), Eq. (12) can be rewritten as

$$\frac{\partial u(\boldsymbol{x})}{\partial \boldsymbol{n}} = \frac{u(\boldsymbol{x}) - u(\tilde{\boldsymbol{x}})}{ds} = \frac{\tilde{\boldsymbol{\varphi}}(\boldsymbol{x}) - \tilde{\boldsymbol{\varphi}}(\tilde{\boldsymbol{x}})}{ds} \boldsymbol{u}_{N_s}. \tag{13}$$

As $\tilde{\boldsymbol{\varphi}}(\boldsymbol{x})$ has the Kronecker-delta property $\tilde{\varphi}_k(\boldsymbol{x}_m) = \delta_{km}$, Eq. (13) can be further modified as

$$\frac{\tilde{\boldsymbol{\varphi}}(\tilde{\boldsymbol{x}}) - \tilde{\boldsymbol{\varphi}}(\boldsymbol{x})}{ds} = \frac{[\tilde{\varphi}_1(\tilde{\boldsymbol{x}}), \ldots, \tilde{\varphi}_k(\tilde{\boldsymbol{x}}) - 1, \ldots, \tilde{\varphi}_N(\boldsymbol{x})]}{ds}, \tag{14}$$

where *k* denotes the node $\boldsymbol{x}_k$ as shown in Fig. 1. In Eq. (14), the field quantity of the only fictitious node is interpolated using the local nodes in the small domain. Due to the Kronecker-delta property, the field quantity at the boundary node is given analytically in the derivative calculation, the accuracy and the stability of the derivative calculation is only related to the interpolation of the field quantity located at the fictitious node. As the distance *ds* is getting smaller, the accuracy of the derivative is greatly increasing in the LRBFCM. This approach combines the advantanges of the RBF interpolation and the Kronecker-delta property together, the derivative can easily be solved no matter how complex is the interface or boundary.

3. The stability tests with a boundary value problem

In order to fully validate the proposed approach, a simple laplace case with a square domain is considered, as shown in Fig. 2. A uniform nodes distribution with 31×31 is considered to compare the proposed approach with the traditional LRBFCM, as shown in Fig.2. The Nuemann boundary condition is considered on right boundary. The shape parameter is fixed with ζ_s =1, the number of local nodes from 5 to 13 are tested as shown in Fig. 3. 9 nearest local nodes are employed including the inner domian and boundary nodes. The exact solutions of $u(x)=sin(x)e^y$ is taken as the test function, numerical errors are given as follows

$$Errors = \sum \left| E_n - E_e \right| / \sum \left| E_e \right|, \tag{15}$$

where the E_e are the exact solution and E_n denote the numerical results. The multiquartic RBF is considered

$$\varphi = \sqrt{r^2 + \zeta_s}$$

where ζ_s is the shape parameter of the RBF and $\zeta_s > 0$.

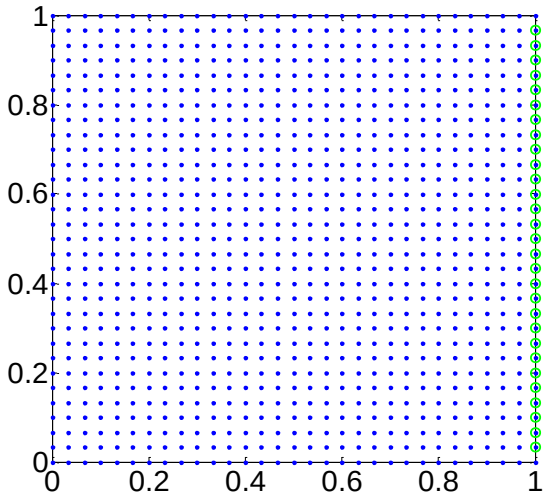

Fig. 2 Uniform nodes distribution

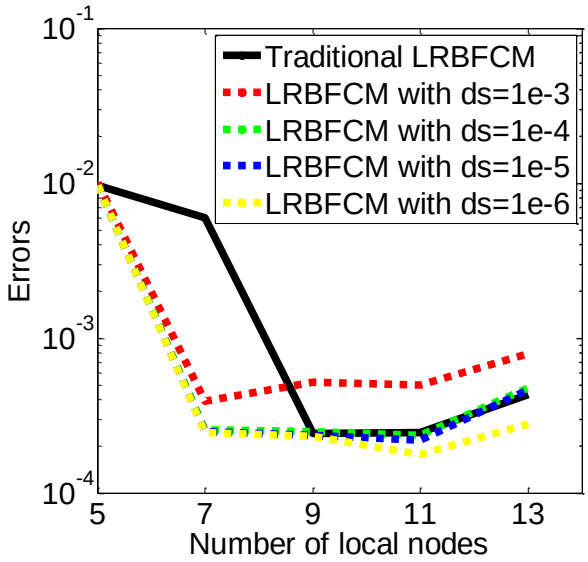

Fig. 3 Comparision of the improved LRBFCM with Traditional LRBFCM

As shown in Fig.3, the convergence rate of the proposed LRBFCM is much faster than traditional LRBFCM, the accuaracy and stability of the proposed LRBFCM increases as the d_s diseases. The numerical results when $d_s=10^{-3}$ show that small value of d_s should be employed to keep a certain accuracy. Theoretically, smaller d_s can always lead to better numerical results. However, singularity may influence numerical results as two nodes are getting close to each other.

In order to show the improvement of the proposed approach, and further discuss the influence of the d_s, the Neumann boundary conditions on all the boundaries, and only one single node information on the right above corner in Fig.4 is given. A disorder with the range of 0.01 is considered based on the same 31×31 uniform nodes to generate the random nodes distribution in Fig.4. The traditional LRBFCM may be difficult to solve this case due to difficulties in choosing

proper shape parameters and subdomain nodes

.

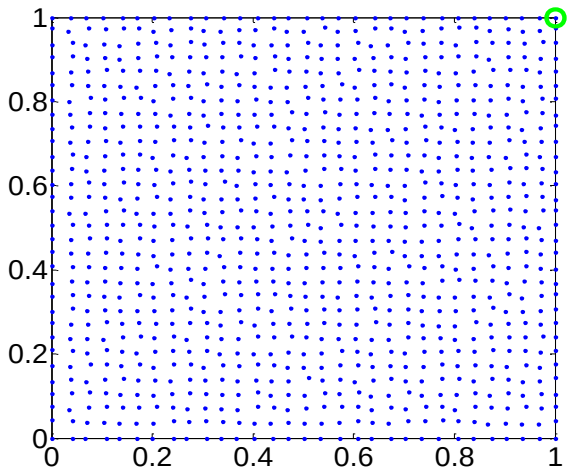

Fig. 4 Nodes distribution of the considered domain

The influence of *ds* with different shape parameters are presented in Fig. 5, where *ds* is changing from 10^{-1} to 10^{-10}. Fig. 5 shows that the *ds* introduced can greatly enhance the LRBFCM for Neumann boundary conditions. As *ds* is decreasing before 10^{-2}, the numerical results are getting better, this is because the accuracy of the of derivative is increasing as *ds* is getting smaller. *ds* between 10^{-2} and 10^{-6} always leads to good results, when *ds* is less than 10^{-8} the numerical results are becoming worse. This is because of the singularity when the nodes are too close.

In general, the proposed numerical approach can well treat the Neumann boundary conditions for LRBFCM, *ds* between 10^{-2} and 10^{-6} is suggested. Based on this approach, the LRBFCM is developed to the phononic crystals with an arbitrary sactterers, where normal derivative in a complex interface must be proper treated.

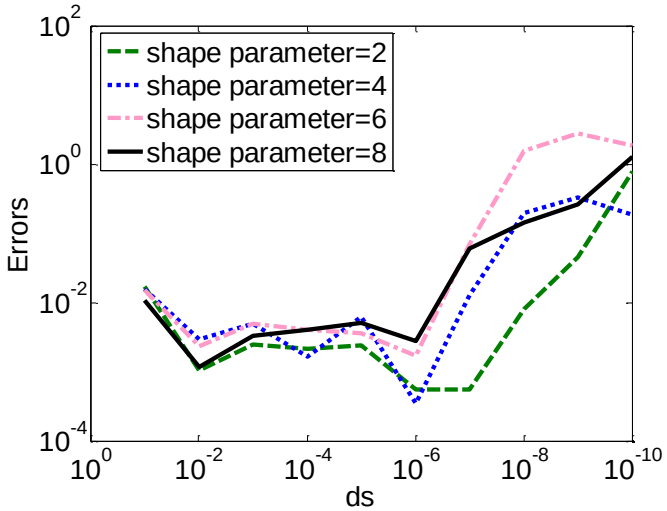

Fig. 5 The numerical results influence with different *ds*

3. Problem of Phononic crystals

Since this work is mainly focus on an arbitrary scatterer phononic crystals, governing equations and related boundary conditions are briefly presented. More the RBF formulation of phononic please refer to [36].

3.1 Governing equations

Consider a 2D phononic crystal composed of scatterers of an arbitrary shape embedded in a square matrix with the lattice constant a as illustrated in Fig. 6, where Γ_1 to Γ_4 and Γ_1 to Γ_6 represent the boundaries of a unit-cell, and Γ_0 is the interface between the matrix and a scatterer. The governing equations of the anti-plane elastic waves in a homogeneous, isotropic and linear elastic solid are

$$\Delta u(\boldsymbol{x}) = -\frac{\omega^2}{c^2} u(\boldsymbol{x}), \tag{16}$$

where ω is the rotation frequency, $c_j = \sqrt{\rho_j / \mu_j}$ the elastic wave speed (j=1 for the scatterer domain D_1 and 2 for the matrix domain D_2), ρ the mass density and μ the shear modulus.

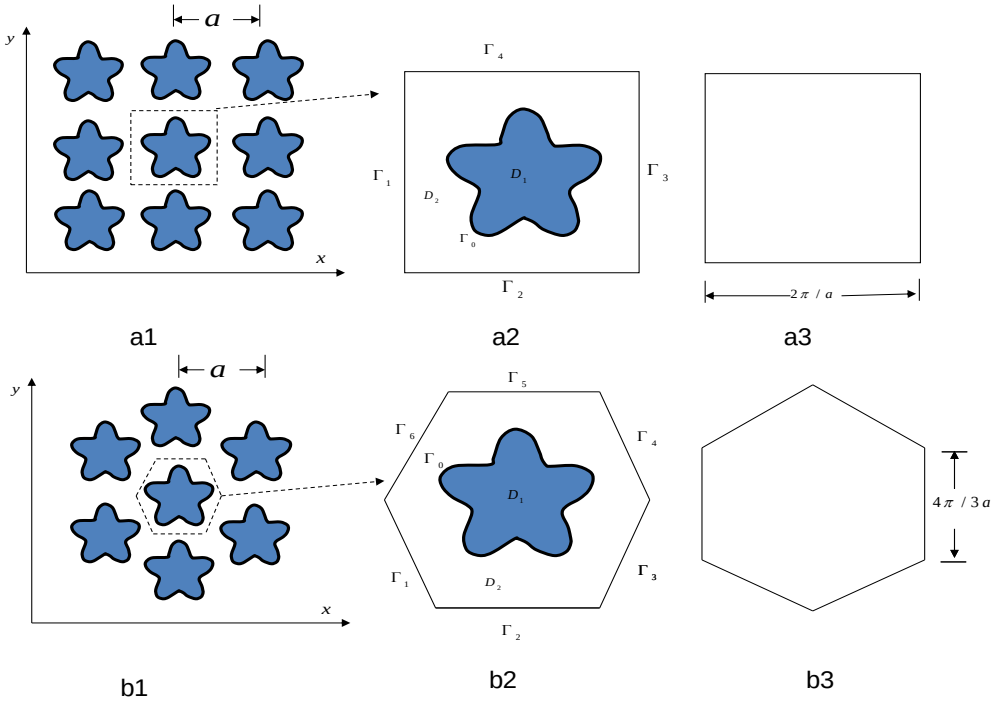

Fig. 6 Phononic crystal structures: (a1), (a2) and (a3) represent the square lattice, the square unit-cell and the first Brillouin zone; (b1), (b2) and (b3) the triangular lattice, the hexagonal unit-cell and the first Brillouin zone.

3.2 Interface conditions

The continuity conditions on the interface Γ_0 are expressed as

$$u^1(\boldsymbol{x}) = u^2(\boldsymbol{x}), \qquad \boldsymbol{x} \in \Gamma_0, \tag{17}$$

$$\mu_1 \frac{\partial u^1(\boldsymbol{x})}{\partial \boldsymbol{n}} = \mu_2 \frac{\partial u^2(\boldsymbol{x})}{\partial \boldsymbol{n}}, \qquad \boldsymbol{x} \in \Gamma_0, \tag{18}$$

where $\boldsymbol{n} = \left(n_x, n_y\right)^T$ is the outward unit normal vector of the scatterer.

3.3 Periodic boundary conditions

The periodic boundary conditions are given as

$$u(\boldsymbol{x} + \boldsymbol{a}) = e^{i\boldsymbol{k}\cdot\boldsymbol{a}} u(\boldsymbol{x}), \tag{19}$$

$$t(\boldsymbol{x} + \boldsymbol{a}) = e^{i\boldsymbol{k}\cdot\boldsymbol{a}} t(\boldsymbol{x}), \tag{20}$$

where $\boldsymbol{k} = (k_x, k_y)^T$ is the Bloch wave vector, $i = \sqrt{-1}$, $t(\boldsymbol{x}) = \dfrac{\partial u(\boldsymbol{x})}{\partial \boldsymbol{n}}$ and $\boldsymbol{a} = l_1\boldsymbol{a}_1 + l_2\boldsymbol{a}_2$ with $(l_1, l_2) \in \mathrm{Z}^2$, where $\boldsymbol{a}_1$ and $\boldsymbol{a}_2$ are fundamental translation vectors of the lattices.

For the square lattice we have

$$u(\boldsymbol{x}_{\Gamma_1} + \boldsymbol{a}) = e^{ik_x a} u(\boldsymbol{x}_{\Gamma_3}), \qquad u(\boldsymbol{x}_{\Gamma_2} + \boldsymbol{a}) = e^{ik_y a} u(\boldsymbol{x}_{\Gamma_4}), \tag{21}$$

$$t(\boldsymbol{x}_{\Gamma_1} + \boldsymbol{a}) = e^{ik_x a} t(\boldsymbol{x}_{\Gamma_3}), \qquad t(\boldsymbol{x}_{\Gamma_2} + \boldsymbol{a}) = e^{ik_y a} t(\boldsymbol{x}_{\Gamma_4}), \tag{22}$$

where $\boldsymbol{x}_{\Gamma_i}$ (i=1~4) are the nodes on the boundaries Γ_i.

For the triangular lattice we have:

$$u(\boldsymbol{x}_{\Gamma_1}) = u(\boldsymbol{x}_{\Gamma_4}) e^{-i\left(k_x \frac{\sqrt{3}}{2} a + k_y \frac{a}{2}\right)}, u(\boldsymbol{x}_{\Gamma_2}) = u(\boldsymbol{x}_{\Gamma_5}) e^{-ik_y a}, u(\boldsymbol{x}_{\Gamma_3}) = u(\boldsymbol{x}_{\Gamma_6}) e^{-i\left(-k_x \frac{\sqrt{3}}{2} a + k_y \frac{a}{2}\right)}, \tag{23}$$

$$t(\boldsymbol{x}_{\Gamma_1}) = t(\boldsymbol{x}_{\Gamma_4}) e^{-i\left(k_x \frac{\sqrt{3}}{2} a + k_y \frac{a}{2}\right)}, t(\boldsymbol{x}_{\Gamma_2}) = t(\boldsymbol{x}_{\Gamma_5}) e^{-ik_y a}, t(\boldsymbol{x}_{\Gamma_3}) = t(\boldsymbol{x}_{\Gamma_6}) e^{-i\left(-k_x \frac{\sqrt{3}}{2} a + k_y \frac{a}{2}\right)}. \tag{24}$$

The generalized eigenvalue matrix can be formulated by substituting Eq. (8) into Eq. (16), Eq. (18), Eq. (22) or Eq. (24). The interface condition Eq. (17) and the periodic boundary condition Eq. (21) or Eq. (23) are considered analytically in the generalized eigenvalue matrix form.

4 Numerical results and discussions

The present LRBFCM is validated by comparison of numerical results with those obtained from finite element modelling using COMSOL™ Multiphysics 5.0. There is little time difference due to different eigenvalue solvers of the LRBFCM and FEM. The generalized eigenvalue equation is

solved numerically by using the eigensolver in MATLAB. 9 local nodes are employed for both boundary and inner domain, $ds=10^{-6}$ is employed, the shape parameter is choosen as 1. Scatterers made of gold (Au) and aluminium (Al) embedded in an epoxy matrix are modelled, respectively. The material constants are $\rho_1=19500 kg/m^3$ and $c_1=1239 m/s$ for Au and $\rho_1=2730 kg/m^3$ and $c_1=3145 m/s$ for Al, respectively. $\rho_2=1180 kg/m^3$ and $c_2=1161 m/s$ for the epoxy. This leads to acoustic impedance ratio $Z=\rho_1 c_1/\rho_2 c_2$ =17.64 for Au and Z=6.46 for Al, respectively.

4.1 Numerical results

Square lattice

The square lattice with a scatterer of star shape and its first Brillouin zone with 225 points are shown on the left and right hand side of Fig. 7 respectively. The band structures are obtained by sweeping all the first Brillouin zone points.

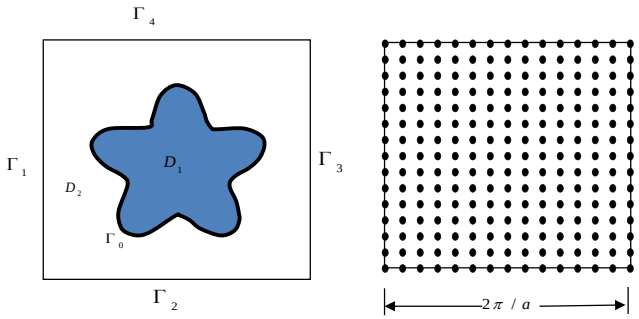

Fig. 7 Square lattice (left) and its related first Brillouin zone (right)

An FE mesh with 2737 degrees of freedom and 1348 elements are used for comparison with the LRBFCM with 2585 degrees of freedom and 2454 nodes, as shown in Fig. 8 and Fig. 9, respectively. The corresponding band structures of the Au scatterer embedded in the epoxy matrix are shown in Fig. 10 and Fig. 11, respectively. It is clear that the present results agree quite well with the FEM results. The band gap can be easily calculated from the first and second band of eigenvalues. Fig. 12 and Fig. 13 show the band structures of the Al scatterer embedded in the epoxy matrix using the FEM and the LRBFCM, respectively. Again an excellent agreement can be seen, and different material properties do not affect the accuracy of numerical results.

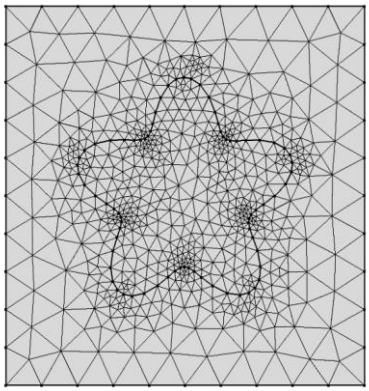

Fig. 8 FEM mesh

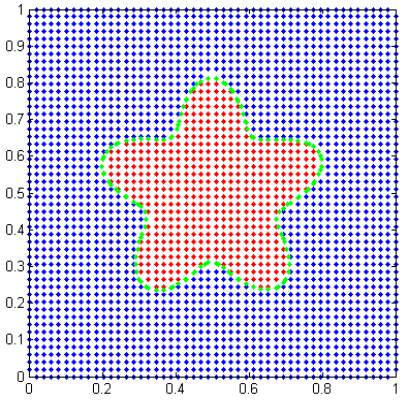

Fig. 9 Nodal distribution in RBF

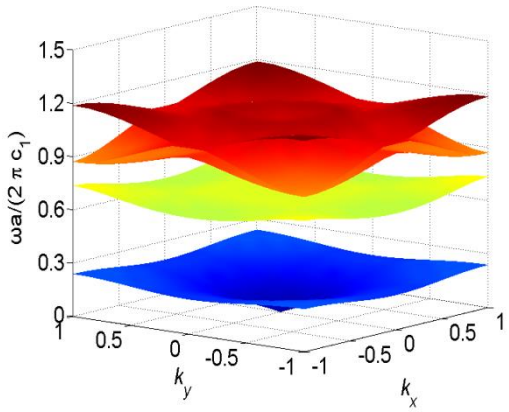

Fig. 10 Band structures of Au/Ep using FEM

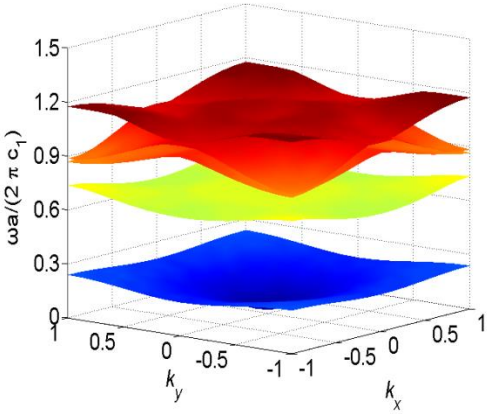

Fig. 11 Band structures of Au/Ep using LRBFCM

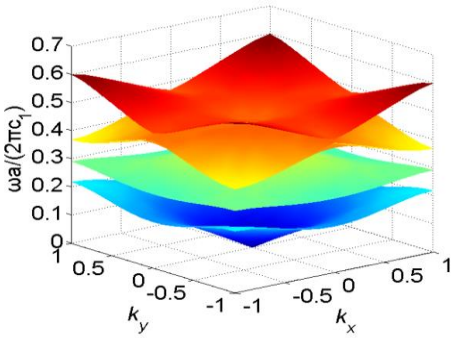

Fig. 12 Band structures of Al/Ep using FEM

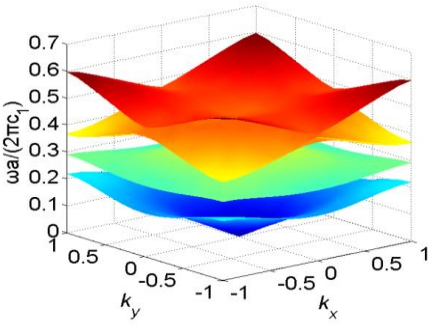

Fig. 13 Band structures of Al/Ep using LRBFCM

Triangular lattice

The triangular lattice with a star shape scatterer is shown in Fig. 14 with 165 points used in the first Brillouin zone. For this example, 1487 degrees of freedom with 408 elements are employed in the FE mesh, and 2181 degrees of freedom with 2055 nodes used in the LRBFCM, as shown in

Fig. 15 and Fig. 16, respectively. Fig. 17 and Fig. 18 show the band structures of the Au scatterer case from the FEM and LRBFCM, respectively. The results for the Al scatterer case are shown in Fig. 19 and Fig. 20, respectively. All the results are in excellent agreement.

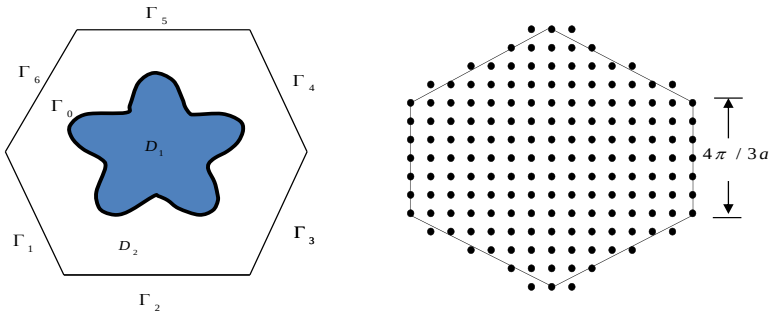

Fig. 14 Triangular lattice (left) and its first Brillouin zone (right)

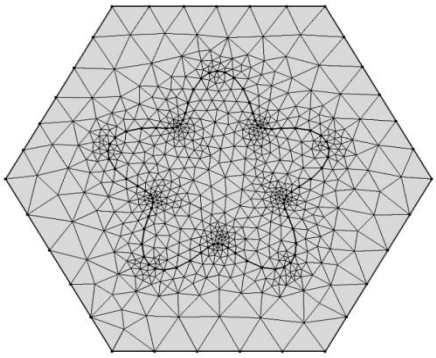

Fig. 15 FEM mesh

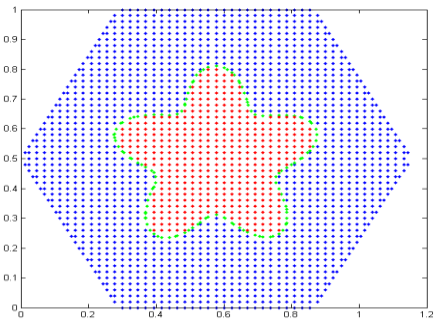

Fig. 16 Nodes distribution in RBF

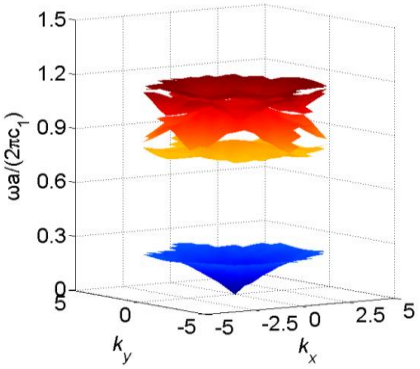

Fig. 17 Band structures of Au/Ep using FEM

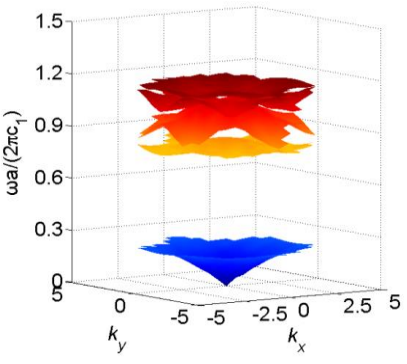

Fig. 18 Band structures of Au/Ep using LRBFCM

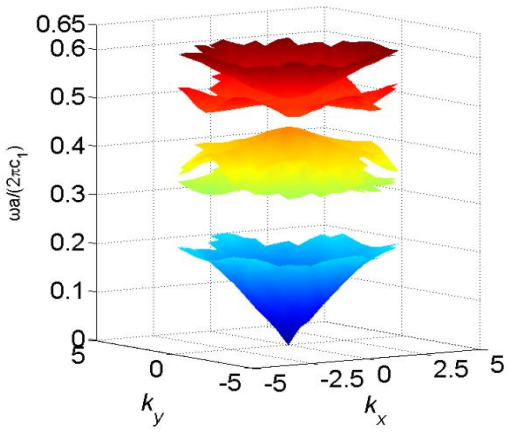

Fig. 19 Band structures of Al/Ep using FEM

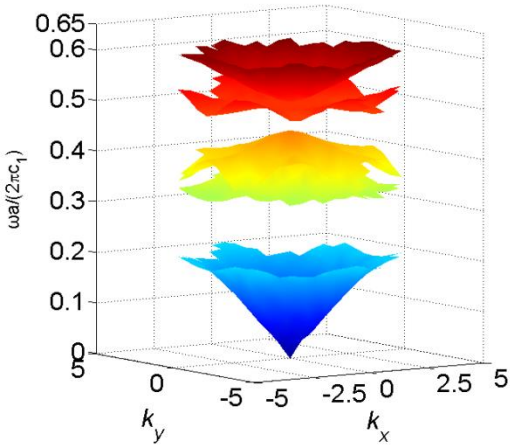

Fig. 20 Band structures of Al/Ep using LRBFCM

4.3 Comparison and analysis

The CPU times and errors of the FEM and the LRBFCM for the above numerical examples are given in Table 1. The lowest ten eigenvalues are compared and the errors are defined as

$$Errors = \sum \left| E_r - E_f \right| / \sum \left| E_r \right|, \tag{25}$$

where E_f is the FEM result using COMSOL™ Multiphysics and E_r the result of LRBFCM implemented in a Matlab code. All the simulations are run on a laptop with Intel(R) Core(TM) i7-4510U, 2.00 GHz CPU and 8 GB RAM.

Table 1 shows that the performance of the LRBFCM is much better than that of the FEM in general. Although more degrees of freedom are purposely employed in the LRBFCM for the examples, the computing time is much less than that required by the FEM, with more than 90% savings in all the cases considered here. The high efficiency of the present LRBFCM is attributed to the fact that it is based on a strong-form formulation of partial differential equations and does not need any numerical integration for computing the system matrices. The errors in Table 1 also shows that the improved LRBFCM can deal with the arbitrary interface very well.

5. Conclusions

In this paper, an improved numerical approach based on the LRBFCM has been developed to accurately compute the normal derivatives of field quantities, and thus the continuity conditions of arbitrary geometry interfaces can be treated more properly, the LRBFCM can be developed to the phononic crystal with scatterers of arbitrary geometry. Numerical results show that the improved LRBFCM is capable of very efficiently computing the band structure of phononic crystals with scatterers of arbitrary geometry. Due to its advantages in dealing with complicated boundary or interface shapes, the improved LRBFCM can be extended to simulate other problems such as acoustics, solid-fluid interaction, crack propagation and hydrodynamics with moving boundaries.

Table 1 Comparisons of computing time and accuracy for the phononic crystals

Lattice form		**Square**		**Triangular**	
Material properties		**Au/Ep**	**Al/Ep**	**Au/Ep**	**Al/Ep**
RBF	Degrees of freedom	2585	2585	2055	2055
	Time spent [s]	88.8	92.24	48.8	52.9
FEM	Degrees of freedom	2055	2055	1487	1487
	Time spent [s]	1003	1130	463	412
Comparison	Errors	0.00698	0.00335	0.00410	0.00205
	Time saving	91.14%	91.84%	96.72%	96.44%

Acknowledgments

This work was undertaken as part of a Post Doctoral Fellowship (H. Zheng) at Coventry University and subsequently developed under a National Natural Science Foundation of China Grant (No. 11702125).

References

[1] Kushwaha MS, Halevi P, Dobrzynski L, Djafarirouhani B. Acoustic band-structure of periodic elastic composites. Physical Review Letters 1993;**71**(13): 2022-2025.

[2] Hou G, Wang J, Layton A. Numerical methods for fluid-structure interaction - A review. Communications in Computational Physics 2012;**12(**2): 337-377.

[3] Axmann W, Kuchment P. An efficient finite element method for computing spectra of photonic and acoustic band-gap materials - I. Scalar case. Journal of Computational Physics 1999;**150**(2): 468-481.

[4] Li JB, Wang YS, Zhang CZ. Dispersion relations of a periodic array of fluid-filled holes embedded in an elastic solid. Journal of Computational Acoustics 2012;**20**(4): 525-541.

[5] Belytschko T, Liu WK, Moran B, Elkhodary K. Nonlinear Finite Elements for Continua and Structures (second edition). In: John Wiley & Sons, Ltd, West Sussex, 2014.

[6] Cao YJ, Hou ZL, Liu YY. Convergence problem of plane-wave expansion method for phononic crystals. Physics Letters A 2004;**327**(2-3): 247-253.

[7] Wu TT, Huang ZG, Lin S. Surface and bulk acoustic waves in two-dimensional phononic crystal consisting of materials with general anisotropy. Physical Review B 2004;**69**(9): 094301(1)-094301(10).

[8] Checoury X, Lourtioz JM. Wavelet method for computing band diagrams of 2D photonic crystals. Optics Communications 2006;**259**(1): 360-365.

[9] Sigalas MM, García N. Importance of coupling between longitudinal and transverse components for the creation of acoustic band gaps: The aluminum in mercury case. Applied

Physics Letters 2000;76(16): 2307-2309.
[10] Sigalas MM, Economou EN. Elastic and acoustic-wave band structure. Journal of Sound and Vibration 1992;**158**(2): 377-382.
[11] Kafesaki M, Economou EN. Multiple-scattering theory for three-dimensional periodic acoustic composites. Physical Review B 1999;60(17): 11993-2001.
[12] Wu YM, Lu YY. Dirichlet-to-Neumann map method for analyzing interpenetrating cylinder arrays in a triangular lattice. Journal of the Optical Society of America B 2008;**25**(9): 1466-1473.
[13] Li FL, Wang YS, Zhang CZ. Bandgap calculation of two-dimensional mixed solid-fluid phononic crystals by Dirichlet-to-Neumann maps. Physica Scripta 2011;**84**(5): 055402-55410.
[14] Li FL, Wang YS, Zhang CZ, Yu GL. Bandgap calculations of two-dimensional solid-fluid phononic crystals with the boundary element method. Wave Motion 2013;**50**(3): 525-541.
[15] Gao H, Xiang J, Zheng C, Jiang Y, Matsumoto T. BEM-based analysis of elastic banded material by using a contour integral method. Engineering Analysis with Boundary Elements 2015;**53**: 56-64.
[16] Gao HF, Matsumoto T, Takahashi T, Isakari H. Analysis of band structure for 2D acoustic phononic structure by BEM and the block SS method. Computer Modeling in Engineering & Sciences 2013;**90**(4): 283-301.
[17] Shi ZJ, Wang YS, Zhang CZ. Band structure calculation of scalar waves in two-dimensional phononic crystals based on generalized multipole technique. Applied Mathematics and Mechanics 2013;**34**(9): 1123-1144.
[18] Shi ZJ, Wang YS, Zhang CZ. Band structure calculations of in-plane waves in two-dimensional phononic crystals based on generalized multipole technique. Applied Mathematics and Mechanics 2015;**36**(5): 557-80.
[19] Wang G, Wen JH, Han XY, Zhao HG. Finite difference time domain method for the study of band gap in two-dimensional phononic crystals. Acta Physica Sinica 2003;**52**(8): 1943-47.
[20] Sun JH, Wu TT. Propagation of acoustic waves in phononic-crystal plates and waveguides using a finite-difference time-domain method. Physical Review B 2007;**76**(10): 104304(1)-104304 (8).
[21] Hart EE, Cox SJ, Djidjeli K. Compact RBF meshless methods for photonic crystal modelling. Journal of Computational Physics 2011;**230**(12): 4910-4921.
[22] Hart EE, Cox SJ, Djidjeli K, Kubytskyi VO. Solving an eigenvalue problem with a periodic domain using radial basis functions. Engineering Analysis with Boundary Elements 2009; **33**(2): 258-262.
[23] Kansa EJ. Multiquadrics - A scattered data approximation scheme with applications to computational fluid dynamics. 1. Computers & Mathematics with Applications 1990;**19**(8-9): 127-45.
[24] Fasshauer GE. Meshfree Approximations with MATLAB. World Scientific Publishers, Singapore. 2007.
[25] La Rocca A. and Power H. A double boundary collocation Hermitian approach for the solution of steady state convection–diffusion problems. Comput. Math. Appl., 55:1950–1960, 2008.
[26] Wright G. and Fornberg B. Scattered node compact finite difference–type formulas generated from radial basis functions. J. Comput. Phys., 212:99–123, 2006.
[27] Shu C., Ding H., and Yeo K. Local radial basis function–based differential quadrature method

and its application to solve two-dimensional incompressible Navier–Stokes equations. Comput. Methods Appl. Mech. Engrg., 192:941–954, 2003.
[28] Martin B, Fornberg B, St-Cyr A. Seismic modeling with radial basis function generated finite differences. Geophysics 2015;**80**(4): T137-T146.
[29] Sarler B, Vertnik R. Meshfree explicit local radial basis function collocation method for diffusion problems. Computers & Mathematics with Applications 2006;**51**(8): 1269-1282.
[30] Vertnik R, Sarler B. Meshless local radial basis function collocation method for convective-diffusive solid-liquid phase change problems. International Journal of Numerical Methods for Heat & Fluid Flow 2006;**16**(5): 617-640.
[31] Liu X., Liu G., Tai K., and Lam K. Radial point interpolation method (RPICM) for partial differential equations. Computers & Mathematics with Applications 2005; **50**:1425–1442.
[32]Bayona, V., Flyer N., Fornberg B. and Barnett G.A., On the role of polynomials in RBF-FD approximations: II. Numerical solution of elliptic PDEs, Journal of Computational Physics 2017; **332**: 257-273.
[33] Martin B. and Fornberg B., Seismic modeling with radial basis function-generated finite differences (RBF-FD) – a simplified treatment of interfaces, Journal of Computational. Physics 2017; **335**: 828-845.
[34] Hart EE, Cox SJ, Djidjeli K. Compact RBF meshless methods for photonic crystal modelling. Journal of Computational Physics 2011;**230**(12): 4910-4921.
[35] Hart EE, Cox SJ, Djidjeli K, Kubytskyi VO. Solving an eigenvalue problem with a periodic domain using radial basis functions. Engineering Analysis with Boundary Elements 2009; **33**(2): 258-262.
[36] Zheng H, Zhang Ch, Wang YS, Sladek J, Sladek V. A meshfree local RBF collocation method for anti-plane transverse elastic wave propagation analysis in 2D phononic crystals. Journal of Computational Physics 2016;**305**: 997-1014.
[37] Zheng H, Zhang Ch, Wang YS, Sladek J, Sladek V. Band structure computation of in-plane elastic waves in 2D phononic crystals by a meshfree local RBF collocation method. Engineering Analysis with Boundary Elements 2016; **66**: 77-90.
[38] Zheng H, Zhang Ch, Wang YS, Chen W, Sladek J, Sladek V. A local RBF collocation method for band structure computations of 2D solid/fluid and fluid/solid phononic crystals. International Journal for Numerical Methods in Engineering 2017; **110**: 467-500.
[39] Michael H, Alain K, Eduardo D. Application of an RBF blending interpolation method to problems with shocks, Computer Assisted Methods in Engineering and Science 2015; **22**: 229–241.
[40] Kee, B.B.T., Liu, G.R. and Lu, C. A least-square radial point collocation method for adaptive analysis in linear elasticity. Engineering Analysis with Boundary Elements 2008; **32**(6): 440-460.
[41] Kee, B.B.T., Liu, G.R. and Lu, C. A regularized least-squares radial point collocation method (RLS-RPCM) for adaptive analysis. Computational Mechanics 2007; **40**(5): 837-853.
[42] Kee, B.B.T., Liu, G.R., Zhang, G.Y. and Lu, C. A residual based error estimator using radial basis functions", Finite Elements in Analysis and Design 2008; **44**(9-10):631-645.
[43] Liu, X., Liu, G., Tai, K. and Lam, K. Radial point interpolation collocation method (RPICM) for the solution of nonlinear Poisson problems. Computational Mechanics 2005; **36**(4): 298-306.
[44] Liu, G.R., Kee, B.B.T. and Chun, L. A stabilized least-squares radial point collocation method (LS-RPCM) for adaptive analysis. Computer Methods in Applied Mechanics and Engineering

2006; **195**(37-40): 4843-4861.
[45] Liu G.R., Meshfree Methods - Moving beyond the finite element method, 1st Edn., 2002, 2nd Edn. 2009, CRC press